Polyhedron 205 (2021) 115292

Contents lists available at ScienceDirect

Polyhedron

journal homepage: www.elsevier.com/locate/poly

Synthesis, characterization and biological studies of a sterically hindered symmetrical nitrogen donor ligand and its metal complexes

C. Shiju [a,*], D. Arish [b], N. Bhuvanesh [c], S. Kumaresan [d]

[a] Synthetic Products Division, Corporate R & D Center, HLL Lifecare Ltd., Akkulam, Trivandrum 695017, India
[b] FunGlass, Alexander Dubček University of Trenčín, Študentská 2, 911 50 Trenčín, Slovakia
[c] Department of Chemistry, Texas A&M University, College Station, TX 77842, USA
[d] Department of Biotechnology, Manonmaniam Sundaranar University, Tirunelveli-627 012, India

ARTICLE INFO

Article history:
Received 15 March 2021
Accepted 22 May 2021
Available online 27 May 2021

Keywords:
Metal complexes
Antimicrobial
DNA binding
Anti-tubercular
Anticancer

ABSTRACT

A new sterically hindered Schiff base ligand (SN-NNDMB) was synthesized from *meso*-1,2-diphenyl ethylenediamine (*meso*-stien) and 4-N,N′-dimethylaminobenzaldehyde. Its structure was determined by single-crystal X-ray diffraction data. The crystal structure of the organic ligand was found to be triclinic, space group *P*-1 with a = 6.1407(8) Å, b = 8.8372(12) Å, c = 12.0006(15) Å, α = 103.882(7)°, β = 95.325(8)°, γ = 91.082(7)°, F(0 0 0) = 254, Dc = 1.253 Mg/m^3, μ = 0.571 mm^{-1}, R = 0.0399, and w*R* = 0.1019. Co, Ni, Cu and Zn complexes of SN-NNDMB were also prepared and characterized by elemental analysis, IR-, mass-, NMR- and electronic- spectra, magnetic moment, molar conductance, powder XRD, and TGA. The obtained results show that the Schiff base ligand acts as a bidentate, coordinated through the azomethine nitrogen atoms. According to the biotest such as Antimicrobial, DNA binding, DNA cleaving, Anti-tubercular, Anticancer, and SOD-like activity, the compounds showed better activity after chelation. The Cu(II)-SN-NNDMB complex showed the highest bioactive potential amonst the analyzed compounds.

1. Introduction

In coordination chemistry, Schiff bases are an essential class of ligands [1–4]. Especially transition metal complexes prepared from such ligands serve various purposes in e.g. biological, clinical, analytical and industrial applications [5–8]. Due to their fascinating architectures and topologies, Schiff base transition metal complexes employing many different metal–ligand combinations have been extensively investigated in recent years. For the biological field in particular, the DNA binding and cleaving ability of a metal complex can be tuned by changing the ligand environment. These studies are also crucial in determining the mechanism of metal ion toxicity [9,10]. It has been reported that a considerable enhancement of the cytotoxicity and a reduction of side the effects of Pt-based drugs can be achievd by modifying them with sterically hindered ligands [11,12]. Although several metal complexes of the aforementioned ligands with fine-tuned electronic and steric structures have been investigated, mostly salen–based complexes [13–16], designing new structures is still of interest, specifically for biochemical and catalysis applications.

In the present study we report the synthesis and characterization of new divalent Co, Ni, Cu, and Zn complexes of a Schiff base derived from the condensation of *meso*-1,2-diphenylethane-1,2-diamine (*meso*-stien) (SN) and 4-N,N′-dimethylaminobenzaldehyde (NNDMB). Biological studies concerning their antimicrobial performance, DNA binding, DNA cleaving, anti-tubercular, anticancerous, or SOD like activity have also been reported.

2. Experimental

2.1. Materials

N,N′-dimethylaminobenzaldehyde was purchased from Sigma-aldrich. Ammonium acetate and benzaldehyde were obtained from Merck. Co, Ni, Cu, and Zn chlorides were Merck samples. The Colon Cancer Cells (HCT116) and human cervical cancer cell line (HeLa) were purchased from National Centre for Cell Science (NCCS), Pune. All the solvents and other reagents were procured from commercial sources and were of analytical grade.

* Corresponding author.
E-mail address: cshiju83@gmail.com (C. Shiju).

https://doi.org/10.1016/j.poly.2021.115292
0277-5387/

2.2. Preparation of meso-1,2-Diphenylethylenediamine (meso-stien)

Ammonium acetate (60.0 g, 0.78 mol) and benzaldehyde (29.0 mL, 0.29 mol) were heated at reflux for 3 h. After allowing the mixture to cool, the white *N*-benzoyl-N′-benzylidine-*meso*-1,2-diphenylethylenediamine was filtered, washed with several portions of ethanol, and dried in a vacuum to achive a yield of 42% (12.0 g). *N*-benzoyl-N′-benzylidine-*meso*-1,2 diphenylethylenediamine (5.0 g, 12 mmol) was treated with 60 mL of 70% H_2SO_4. The mixture immediately turned to a pale red colour. After refluxing for 1 h, the mixture turned black. The hot mixture was poured into a 600 mL beaker filled with crushed ice. After repeated extractions with diethyl ether, the mixture was made alkaline with NaOH. The resulting solution was extracted with dichloromethane. The obtained organic layer was collected, dried over anhydrous magnesium sulfate, and filtered. Stripping CH_2Cl_2 from the mix resulted in *meso*-1,2 diphenylethylenediamine(*meso*-stien) in the form of a pale yellow solid. The yield was found to be ~ 60% (1.57 g) [17,18]. IR (KBr, cm^{-1}) ν: 3337, 3264 (N—H); 1581 (NH_2) (out-of-plane), 684. ^{1}H NMR ($CDCl_3$,), δ:, 1.34 (s NH_2); 3.98 (s CH); ~7.30 (m Ar-CH).

2.3. Synthesis of Schiff base ligand (SN-NNDMB)

A mixture of *meso*-1,2-diphenylethylenediamine (*meso*-stien) (5 mmol, 1.06 g) in MeOH (25 mL) was taken in a 100 mL RB flask. A solution of 4-N,N′-dimethylaminobenzaldehyde (10 mmol, 1.49 g) in MeOH (25 mL) was then added slowly. The reaction mixture was vigorously mixed for about 5 h. The formed precipitate was collected by vacuum filtration and then washed several times using anhydrous ether and dried using a desiccator containing anhydrous $CaCl_2$. The purity of the ligand was analyzed by TLC. The isolated yield of the ligand was found to be ~ 70% (1.66 g). Light yellow crystals, ^{1}H NMR ($CDCl_3$) δ: 7.8 (s CH = N), 2.9 (s, N-$(CH_3)_2$), 6.6–7.5 (m, ArH), 4.6 (s, CH-N). IR (KBr, cm-1) ν: 1605 (C═N), 1367 (C—N), 1444 (N-CH_3), 3025 (Ar CH). Anal. calcd for $C_{32}H_{34}N_4$: C 80.98, H 7.22, N 11.80; found: C 81.21, H 6.85, N 12.12. UV–vis (CH_2Cl_2): λ/nm 328, 402. Mass: *m*/*z* 475.

2.4. Synthesis of metal complexes

The Schiff base (SN-NNDMB) (2 mmol, 0.95 g) in MeOH (20 mL) was taken in a 100 mL RB flask. A solution of metal(II) chloride (1 mmol) in MeOH solution (10 mL) was then added dropwise and the reaction mixture was stirred for 6 h. The volume of the reaction mixture was reduced to ½ of the starting volume under reduced pressure. The formed precipitate was filtered out, washed several times with ether and with a little cold EtOH, followed by dried in a vacuum over anhydrous $CaCl_2$.

[$Co(SN\text{-}NNDMB)_2Cl_2$]

Green, yield ~ 60% (0.65 g) Anal. Calcd. for $C_{64}H_{68}Cl_2CoN_8$: C, 71.23, H, 6.35, N, 10.38, Cl, 6.57, Co, 5.46; Found: C, 70.87, H, 6.07, N, 11.14, Cl, 6.46, Co, 5.35. FAB-Mass: *m*/*z* 1078 [M + 1]. IR (KBr, cm^{-1}) m: 1587, 1445, 3199, 419 cm^{-1}. UV–Vis. (CH_2Cl_2): λ/nm, 530–655. μ_{eff} (BM) = 5.04; Molar conductance (Λc(Ohm^{-1} cm^2mol^{-1}) 11.8.

[$Ni(SN\text{-}NNDMB)_2Cl_2$]

Yellow, yield ~ 68% (0.73 g) Anal. Calcd. for $C_{64}H_{68}Cl_2NiN_8$: C, 71.25, H, 6.35, N, 10.39, Cl, 6.57, Ni, 5.44; Found: C, 71.82, H, 6.24, N, 10.56, Cl, 6.22, Ni, 5.25. ESI-Mass: *m*/*z* 1077 [M + 1]. IR (KBr, cm^{-1}) m: 1576, 1454, 3173, 414 cm^{-1}. UV–Vis. (CH_2Cl_2): λ/nm, ~1100, 640, 385. μ_{eff} (BM) = 3.11; Molar conductance (Λc (Ohm^{-1} cm^2mol^{-1}) 12.2.

[$Cu(SN\text{-}NNDMB)_2Cl_2$]

Blue, yield ~ 64% (0.69 g) Anal. Calcd. for $C_{64}H_{68}Cl_2CuN_8$: C, 70.93, H, 6.32, N, 10.34, Cl, 6.54, Cu, 5.86; Found: C, 70.42, H, 6.62, N, 10.88, Cl, 6.16, Cu, 6.03. FAB-Mass: *m*/*z* 1082 [M + 1]. IR (KBr, cm^{-1}) m: 1574, 1453, 3194, 463 cm^{-1}. UV–Vis. (CH_2Cl_2): λ/nm, ~690. μ_{eff} (BM) = 1.96; Molar conductance (Λc(Ohm^{-1} cm^2-mol^{-1}) 14.4.

[$Zn(SN\text{-}NNDMB)_2Cl_2$]

Light Yellow, yield ~ 65% (0.70 g) Anal. Calcd. for $C_{64}H_{68}Cl_2ZnN_8$: C, 70.81, H, 6.31, N, 10.32, Cl, 6.53, Zn, 6.02; Found: C, 71.21, H, 6.52, N, 10.44, Cl, 6.34, Zn, 5.87. FAB-Mass: *m*/*z* 1083 [M + 1]. IR (KBr, cm^{-1}) m: 1588, 1438, 3235, 453 cm^{-1}. μ_{eff} (BM) = Dia; Molar conductance (Λc(Ohm^{-1} cm^2mol^{-1}) 8.2.

2.5. Physical measurementss

Elemental analysis was performed using a Perkin-Elmer elemental analyzer. The molar conductivity of the complexes was measured in DMSO (10^{-3} M) solutions using a Coronation Digital Conductivity Meter. The electrospray (ESI) mass spectra were recorded using a THERMO Finnigan LCQ Advantage max ion trap mass spectrometer. Samples of 10 μL dissolved in methanol, chloroform or dichloromethane were introduced into the ESI source using Finnigan surveyor autosampler and FAB mass spectra were acquired using a JEOL JMS600H mass spectrometer. ^{1}H NMR spectra were obtained using a JEOL GSX 400 FT–NMR spectrometer. IR spectra were recorded using a JASCO FT/IR-410 spectrometer in the 4000–400 cm^{-1} region. Electronic spectra were acquired using a Perkin Elmer Lambda-25 UV–VIS spectrometer. Cyclic voltammetric measurements were acquired using a Bio-Analytical System (BAS) model CV-50 W electrochemical analyzer. Magnetic measurements were performed on a Guoy balance by making diamagnetic corrections using Pascal's constant. The three-electrode cells contain a Ag/AgCl reference, an auxiliary Pt and working glassy electrodes. Tetrabutylammonium perchlorate was used as a supporting electrolyte. Thermal analysis was performed using a SDT Q 600/V8.3 build 101 thermal analyzer with a heating rate of 20 ^{0}C/min in a N_2 atmosphere. Powder XRD was performed on a Rigaku Dmax X-ray diffractometer using Cu-Kα radiation.

A BRUKER GADDS X-ray diffractometer was employed for single crystal screening, unit cell determination, and data collection. The detailed method of data reduction, structure solution, and refinement was reported in Ref. [19].

2.6. Antimicrobial activities

The antimicrobial efficacy of the synthesized compounds was tested in vitro against the bacterial species *Escherichia coli, Pseudomonas aeruginosa, Bacillus subtilis,* and *Staphylococcus aureus* as well as the fungal species *Aspergillus niger, Aspergillus flavus*, and *Candida albicans* using the disc diffusion method. Amikacin, ofloxacin and ciprofloxacin were used as standards for antibacterial activity and nystatin was used as a standard for the antifungal activity. The detailed procedure was reported in Ref. [20].

2.7. DNA binding studies

2.7.1. Absorption titration experiment

Electronic absorption titrations were performed in a Tris-HCl/NaCl buffer (5 $mmolL^{-1}$ Tris-HCl/50 $mmolL^{-1}$ NaCl buffer pH 7.2)

using a DMF (10%) solution of metal complexes at room temperature. The concentration of CT-DNA was determined from the absorption intensity at 260 nm with an ε value of 6600 ($molL^{-1}$)-$^{-1}cm^{-1}$. Absorption titration experiments were made using different concentrations of CT-DNA while keeping the complex concentration constant. The correction was made for the absorbance of the CT-DNA itself. Metal-DNA solutions were allowed to incubate for 5 min before the absorption spectra were recorded. For metal(II) complexes, the intrinsic binding constant (K_b) was determined by monitoring the changes of the absorption in the MLCT band with increasing concentrations of DNA using the following equation.

$[DNA]/(\varepsilon_a-\varepsilon_f) = [DNA]/(\varepsilon_b-\varepsilon_f) + 1/K_b(\varepsilon_b-\varepsilon_f)$where [DNA] means the concentration of DNA in the base pairs. The apparent absorption coefficients ε_a, ε_f and ε_b correspond to A_{obsd}/[Complex], the extinction coefficient of the complex when fully bound to equilibrium binding constant in $(molL^{-1})^{-1,}$ respectively. Each sample solution was scanned from 200 to 500 nm.

2.7.2. Viscosity measurements

Viscosity experiments were performed using an Ostwald viscometer immersed in a thermostated water-bath maintained at a constant temperature at 30 ± 0.1 °C. DNA samples of approximately 0.5 mM were prepared by sonicating to minimize complexities arising from the DNA flexibility. The flow time was monitored with a digital stopwatch three times for each sample and an average flow time was calculated. Each experiment was repeated three times and an average flow time was calculated. The data were represented as $(\eta/\eta_0)^{1/3}$ versus binding ratio, where η is the viscosity of DNA in the presence of complex and η_0 is the viscosity of the pure DNA. Viscosity values were calculated after correcting the flow time with that of the pure buffer (t_0), $\eta = (t - t_0)/t_0$.

The testing procedures for DNA cleavage, in vitro anticancer activity, and MTT assay was followed as reported in the Refs. [20] and [21].

2.8. Antimycobacterial activity screening by resazurin microplate assay (REMA)

The anti-tuberculosis efficacy of the synthesized compounds was tested by the resazurin microplate assay (REMA) as reported by Martin et al., [22] with slight modification. The mechanism is based on a redox dye color change, namely Resazurin, from blue in the oxidized form to pink in the reduced for resorufin which is triggered by the presence of viable cells. Mycobacterium tuberculosis H37Rv was grown in a Middlebrook 7H9 broth (Difco BBL, Sparks, MD, USA) with additions of 10% Oleic Acid Albumin Dextrose Complex and 0.5% glycerol. The microbial culture optical density was adjusted to the McFarland 1.0 unit and 50 μL from this suspension were used as the inoculum. Stock solutions (prepared compounds) were prepared in dimethylformamide (DMF) and were added to a fresh medium in the wells of a microplate to which 50 μL inoculum was added, making the total assay volume 200 μL. The resulting concentrations of the test compounds were 1, 10 and 100 μg/mL. Growth control wells contained the M. tuberculosis H37Rv and medium alone. 1.0 μg/mL of Rifampicin was used as a positive control to inhibit growth, and negative control wells contained the highest volume of DMF used in test wells without any compound. The test microplate was incubated for 7 days at 37 °C, then 15 μL of 0.01% a resazurin solution in sterile water was added to the first growth control wells and again incubated for one day. After the first set of growth controls turned pink, the procedure was repeated, i.e. the dye solution was added to the second set of growth controls and test wells and incubated for 24 h at 37 °C. If the blue color retained in the wells containing the test compounds would indicate growth inhibition, the pink would indicate a lack of growth inhibition for M. tuberculosis [23].

2.9. SOD activity

In vitro Superoxide dismutase (SOD) activity was measured using DMSO as a source of superoxide radicals (O^{2-}) and nitrobluetetrazolium (NBT) as the O^{2-} scavenger. In the general procedure, a 400 mL sample to be evaluated was added to a solution of 2.1 mL potassium phosphate buffer (0.2 M, pH 8.6) and 1 mL of NBT (56 mM). The test tubes were accumulated in an ice tank for 15 min, and then 1.5 mL of alkaline DMSO solution was added and stirred well. The absorbance at 540 nm was examined against a solution prepared under similar conditions without adding NaOH to the DMSO. A unit of SOD activity is the concentration of a complex or enzyme, which causes a 50% inhibition of the alkaline dimethylsulphoxide (DMSO) mediated reduction of NBT.

3. Results and discussion

3.1. Characterization of Schiff base ligand (SN-NNDMB)

The Schiff base ligand SN-NNDMB shows a pale yellow and is soluble in all common organic solvents. The elemental analysis data presented in Table 1 of the ligand is in good agreement with those calculated for the suggested formula. In the ^1H NMR ($CDCl_3$) spectrum, the two azomethine protons exhibit a singlet at 7.8 ppm and the aromatic protons appear in the 6.6–7.5 ppm range. The four methyl groups in the ligand cause a singlet at 2.9 ppm while the protons adjacent to the azomethine nitrogen cause one at at 4.6 ppm. The SN-NNDMB mass spectrum shows a well-defined molecular ion peak at m/z = 475 (relative intensity = 100%), which coincides with the Schiff base formula weight (Fig. 1). A peak at m/z 432 corresponds to $M^{+\cdot}$ –$(CH_3\text{-}N\text{-}CH_3)^{\cdot}$ and is presented in Scheme 1. In the UV spectrum of SN-NNDMB, the absorption bands at 328 and 402 nm can be attributed to the π–π* transitions of the azomethine chromophore. The IR (KBr) spectrum presented in Table 2 of the Schiff base ligand SN-NNDMB exhibits a band at 1605 cm^{-1} due to azomethine group ν(C=N).

3.2. Crystallographic study

Single-crystal XRD data and structure refinement for the ligand is shown in Table 3. The organic ligand crystallized in the triclinic space group *P*-1 with a = 6.1407(8) Å, b = 8.8372(12) Å, c = 12.0006 (15) Å, α = 103.882(7)°, β = 95.325(8)°, γ = 91.082(7)°, V = 628.91 (14) Å3, Z = 1, F(0 0 0) = 254, D_c = 1.253 Mg/m^3, μ = 0.571 mm^{-1}, R = 0.0399, and w*R* = 0.1019. Key bond angles and bond lengths are shown in Tables 4a and 4b and are all within the normal range. The ORTEP diagram of the ligand molecule SN-NNDMB is shown in Fig. 2a. The crystal data shows that the two phenyl rings and two azomethane nitrogens are *trans* oriented as shown by the torsion angle values C1–C7–C7a–C1a = 180° and N1–C7–C7a–N1a = 180°. The packing structures and two-dimensional structures of the ligand SN-NNDMB are shown in Fig. 2b. The single-crystal X-ray diffraction study confirmed the formation of the Schiff base SN-NNDMB.

3.3. Characterization of metal Schiff base complexes

The analytical and physical characterization of the M(II)-SN-NNDMB complexes are shown in Table 1. The elemental analysis results show that the metal-to-ligand ratio is 1:2 in all the complex systems. The composition of the complexes is [$M(SN\text{-}NNDMB)_2$-Cl_2]. The low molar conductance values (see Table 2) of the metal

Table 1
Analytical and physical data of SN-NNDMB and its complexes.

Compound	Empirical formula	Colour	yield	Elemental analysis Found (calcd) %				
				C	H	N	Cl	M
SN-NNDMB	$C_{32}H_{34}N_4$	Light Yellow	75%	81.21 (80.98)	6.85 (7.22)	12.12 (11.80)	–	–
$[Co(SN\text{-}NNDMB)_2Cl_2]$	$C_{64}H_{68}Cl_2CoN_8$	Green	60%	70.87 (71.23)	6.07 (6.35)	11.14 (10.38)	6.46 (6.57)	5.35 (5.46)
$[Ni(SN\text{-}NNDMB)_2Cl_2]$	$C_{64}H_{68}Cl_2NiN_8$	Yellow	68%	71.82 (71.25)	6.24 (6.35)	10.56 (10.39)	6.22 (6.57)	5.25 (5.44)
$[Cu(SN\text{-}NNDMB)_2Cl_2]$	$C_{64}H_{68}Cl_2CuN_8$	Blue	64%	70.42 (70.93)	6.62 (6.32)	10.88 (10.34)	6.16 (6.54)	6.03 (5.86)
$[Zn(SN\text{-}NNDMB)_2Cl_2]$	$C_{64}H_{68}Cl_2ZnN_8$	Light Yellow	65%	71.21 (70.81)	6.52 (6.31)	10.44 (10.32)	6.34 (6.53)	5.87 (6.02)

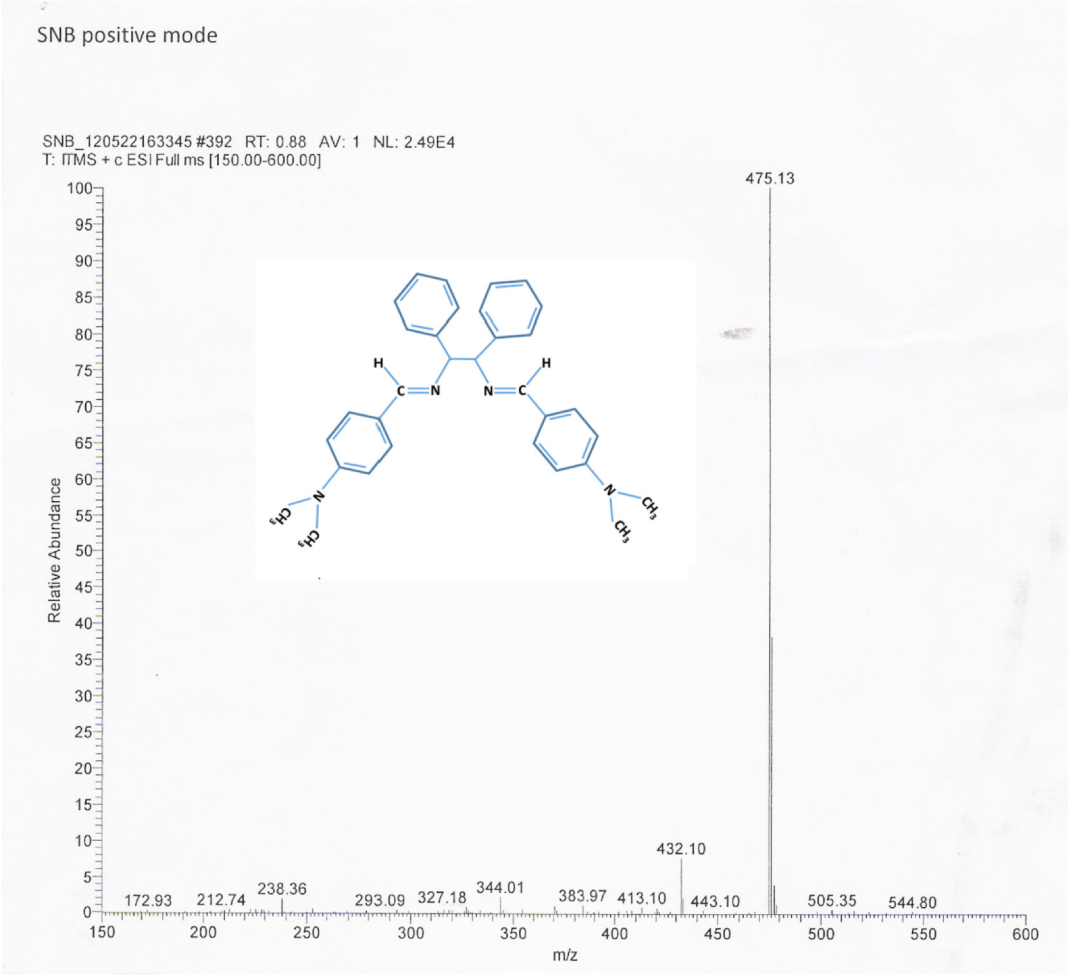

Fig. 1. Mass spectrum of SN-NNDMB.

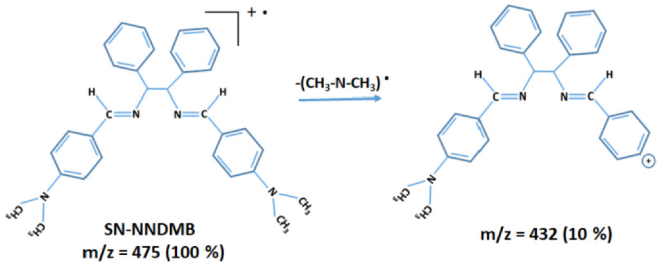

Scheme 1. Mass fragmentation.

complexes reveal their non-electrolytic nature. The $[Co(SN\text{-}NNDMB)_2Cl_2]$, $[Ni(SN\text{-}NNDMB)_2Cl_2]$, $[Cu(SN\text{-}NNDMB)_2Cl_2]$ and $[Zn(SN\text{-}NNDMB)_2Cl_2]$ complexes are soluble in methanol, chloroform, dichloromethane, DMF, DMSO.

The mass spectra of the $[Co(SN\text{-}NNDMB)_2Cl_2]$, $[Ni(SN\text{-}NNDMB)_2Cl_2]$, $[Cu(SN\text{-}NNDMB)_2Cl_2]$ and $[Zn(SN\text{-}NNDMB)_2Cl_2]$ complexes show molecular ion peaks at *m/z* 1078 (25%), 1077 (100%), 1082 (18%), and 1083 (14%), respectively, which coincide with the formula weights of the Schiff base complexes.

3.4. IR spectra

Selected IR spectral data are stated in Table 2. The band at 1605 cm^{-1} for the azomethine group of the free ligand was shifted to a lower frequency in the range from ~1574 to 1588 cm^{-1} in the complexes indicating the coordination of the azomethine N atom to the metal center. There is no broadband near 3400 cm^{-1}, indicating the absence of water molecules. The IR spectra of all the

Table 2
IR, conductance, and magnetic moment and UV data of SN-NNDMB and its complexes.

Compound	IR cm^{-1}		$\Lambda c(Ohm^{-1}\ cm^2 mol^{-1})$	$\mu_{eff\ (B.M)}$	UV/Vis nm
	$\nu_{azo.}(C{=}N)$	$\nu(M{-}N)$			
SN-NNDMB Ligand	1605	–		–	328, 402
$[Co(SN\text{-}NNDMB)_2Cl_2]$	1587	419	11.8	5.04	530–655
$[Ni(SN\text{-}NNDMB)_2Cl_2]$	1576	414	12.2	3.11	~1100, 640, 385
$[Cu(SN\text{-}NNDMB)_2Cl_2]$	1574	463	14.4	1.96	~690
$[Zn(SN\text{-}NNDMB)_2Cl_2]$	1588	453	8.2	Dia	–

Table 3
Crystal data and structure refinement for SN-NNDMB.

	SN-NNDMB	
CCDC	2020181	
Empirical formula	C32 H34 N4	
Formula weight	474.63	
Temperature	110(2) K	
Wavelength	1.54178 Å	
Crystal system	Triclinic	
Space group	P-1	
Unit cell dimensions	a = 6.1407(8) Å	α = 103.882 (7)°
	b = 8.8372(12) Å	β = 95.325(8)°
	c = 12.0006(15) Å	γ = 91.082(7)°
Volume	628.91(14) Å3	
Z	1	
Density (calculated)	1.253 Mg/m3	
Absorption coefficient	0.571 mm-1	
F(000)	254	
Crystal size	0.06 x 0.03 x 0.02 mm3	
Theta range for data collection	3.81 to 59.99°.	
Index ranges	-6<=h<=6, -9<=k<=9, -13<=l<=13	
Reflections collected	5421	
Independent reflections	1737 [R(int) = 0.0336]	
Completeness to theta = 59.99°	93.2 %	
Absorption correction	Semi-empirical from equivalents	
Max. and min. transmission	0.9887 and 0.9665	
Refinement method	Full-matrix least-squares on F2	
Data/restraints/parameters	1737/0/165	
Goodness-of-fit on F2	1.004	
Final R indices [I>2sigma(I)]	R1 = 0.0399, wR2 = 0.1019	
R indices (all data)	R1 = 0.0556, wR2 = 0.1085	
Largest diff. peak and hole	0.155 and -0.189 e.Å-3	

Table 4a
Selected bond lengths.

Bond	Bond Lengths
N(1)-C(8)	1.277(2)
N(1)-C(7)	1.472(2)
N(2)-C(12)	1.376(2)
N(2)-C(15)	1.442(2)
N(2)-C(16)	1.449(2)
C(1)-C(6)	1.387(2)
C(1)-C(2)	1.395(3)
C(1)-C(7)	1.516(2)
C(7)-C(7)#1	1.534(3)
C(12)-C(13)	1.402(3)
C(13)-C(14)	1.389(3)
C(2)-C(3)	1.393(3)
C(3)-C(4)	1.377(3)
C(4)-C(5)	1.387(3)
C(5)-C(6)	1.388(3)
C(9)-C(14)	1.390(2)
C(9)-C(10)	1.401(3)
C(10)-C(11)	1.379(3)
C(11)-C(12)	1.411(3)

Table 4b
Selected Bond Angles (°).

Bond	Bond Angles (°)
C(8)-N(1)-C(7)	116.58(15)
C(12)-N(2)-C(15)	120.45(15)
C(12)-N(2)-C(16)	120.73(16)
C(15)-N(2)-C(16)	117.62(15)
C(6)-C(1)-C(2)	118.43(17)
C(6)-C(1)-C(7)	121.85(16)
C(2)-C(1)-C(7)	119.65(17)
C(3)-C(2)-C(1)	120.53(19)
C(4)-C(3)-C(2)	120.20(18)
C(3)-C(4)-C(5)	119.89(17)
C(4)-C(5)-C(6)	119.82(19)
C(1)-C(6)-C(5)	121.12(18)
N(1)-C(7)-C(1)	108.33(14)
N(1)-C(7)-C(7)#1	108.78(17)
C(1)-C(7)-C(7)#1	113.51(17)
N(1)-C(8)-C(9)	124.31(17)
C(14)-C(9)-C(10)	118.09(16)
N(2)-C(12)-C(13)	121.94(16)
N(2)-C(12)-C(11)	120.61(17)
C(3)-C(12)-C(11)	117.45(16)

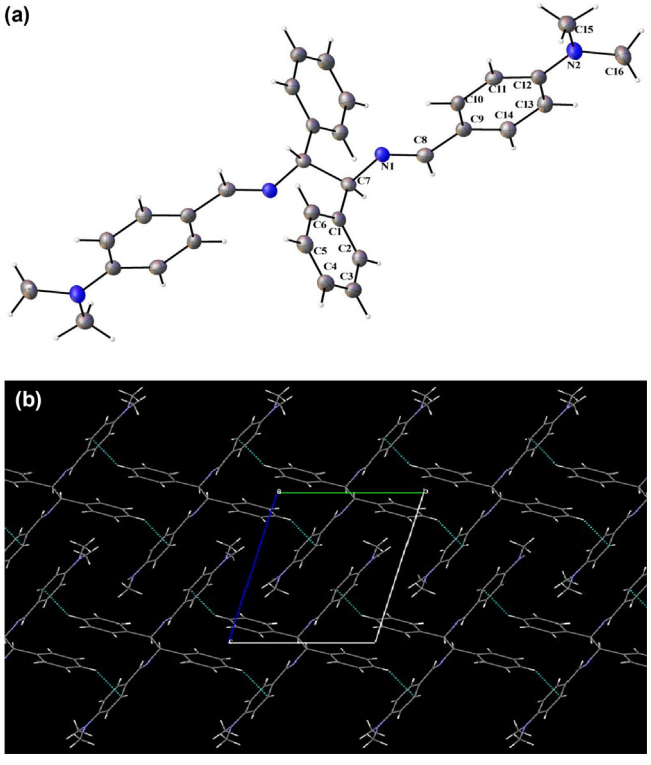

Fig. 2. a. ORTEP diagram of the Schiff base SN-NNDMB b. Packing Structure of the Schiff base SN-NNDMB along an axis.

metal complexes show new bands in the 429–465 cm^{-1} region, probably due to M—N bond formation.

3.5. Electronic spectra and magnetic properties

The electronic spectrum of $[Co(SN\text{-}NNDMB)_2Cl_2]$ complexes show two absorption bands (see Table 2) in the 530–655 nm region, which can be assigned to the overlap of $^4T_1g(F)\rightarrow{}^4A_2g(F)$ and $^4T_1g(F)\rightarrow{}^4T_2g(F)$ transitions in an octahedral environment [24]. The electronic spectrum of the $[Ni(SN\text{-}NNDMB)_2Cl_2]$ complex shows three bands in the regions around 385, 640 and ~1100 nm attributable to $^3A_2g(F)\rightarrow{}^3T_1g(P)$, $^3A_2g(F)\rightarrow{}^3T_1g(F)$ and $^3A_2g(F)\rightarrow{}^3T_2g(F)$ transitions, respectively, suggesting an octahedral geometry around the Ni(II) atom [24]. The $[Cu(SN\text{-}NNDMB)_2Cl_2]$ complex in its spectrum displays a broadband in the ~ 690 nm region, which can be assigned to an $^2Eg\rightarrow{}^2T_2g$ transition, indicating that the complex has a distorted octahedral geometry [24]. The magnetic susceptibility value is 5.04 BM for $[Co(SN\text{-}NNDMB)_2Cl_2]$ (the normal range for octahedral Co(II) complexes is 4.3–5.2 BM), again indicating a octahedral geometry of the complex [25]. The $[Ni(SN\text{-}NNDMB)_2Cl_2]$ complex reported herein is found to have a room temperature magnetic moment value of 3.11 BM, which is in the normal range observed for octahedral Ni(II) complexes (μeff 2.9 – 3.3 BM) [25]. The magnetic moment value of the $[Cu(SN\text{-}NNDMB)_2Cl_2]$ complex is 1.96 BM which is also normal to observe for octahedral Cu(II) complexes [25].

3.6. Thermal analysis

Table 5 showes the thermal stability data of the complexes. The $[Co(SN\text{-}NNDMB)_2Cl_2]$, $[Ni(SN\text{-}NNDMB)_2Cl_2]$, $[Cu(SN\text{-}NNDMB)_2Cl_2]$, and $[Zn(SN\text{-}NNDMB)_2Cl_2]$ complexes undergo the same type of decomposition. The decomposition step is represented by a complete removal of the organic ligand moiety in the 250–800 °C range with the formation of a metal oxide as the final product. The TG curves of the complex $[Co(SN\text{-}NNDMB)_2Cl_2]$ show a weight loss of 93.45% (calculated – 93.05%) in the temperature range from 260 to 545 °C which is due to the decomposition of the coordinated organic ligand. Above this temperature, a horizontal thermal curve is observed due to the metal oxide formation. The TG curves of the complexes $[Ni(SN\text{-}NNDMB)_2Cl_2]$ show a weight loss 92.75% (93.06%) in the temperature range from 300 to 690 °C showing the elimination of the coordinated organic ligand. Above this temperature, there is no noticeable weight loss. The complexes $[Cu(SN\text{-}NNDMB)_2Cl_2]$ and $[Zn(SN\text{-}NNDMB)_2Cl_2]$ show similar decomposition trends. The decomposition in the temperature range from 290 to 700 °C for the $[Cu(SN\text{-}NNDMB)_2Cl_2]$ and 275–800 °C for $[Zn(SN\text{-}NNDMB)_2Cl_2]$ complexes correspond to the decomposition of the organic ligand molecule and it is in agreement with the calculated mass loss. The final residue is qualitatively proved to be composed of anhydrous metal oxides.

3.7. Electrochemical studies

Cyclic voltammetry offers a rapid location of redox potentials of the electroactive species, especially for acquiring qualitative information about electrochemical reactions. The cyclic voltammograms of metal complexes were recorded at 300 K in the DMSO solution and the potential range from −1.0 to 1.2 V with a CT scan rate of 0.1 V/s. The Co(II) complex shows two peaks; one at E_{pc} = 0.90 V corresponding to a Co(II)/(I) couple and another at E_{pc} = -0.15 V during the reverse scan corresponding to a Co(II)/(III) couple. The peak to peak separation ΔE is 0.75 V indicating the process to be irreversible. The Ni(II) complex shows two irreversible peaks, one at E_{pc} = 0.70 V and another at E_{pc} = 0.40 V corresponding to a Ni(II)/(I) couple. The Cu(II) complex shows a cathodic peak at E_{pc} = 0.5 V vs Ag/AgCl corresponding to a Cu(II)/(III) couple and the associated anode peak at E_{pa} = -0.6 V corresponding to the formation of a Cu(II)/I couple. The peak to peak separation ΔE is 1.10 V confirming the process to be irreversible. The Zn(II) complex shows a peak at E_{pc} = 0.40 V vs Ag/AgCl and the associated anode peak at E_{pa} = 0.55 V. The peak to peak separation value ΔE = 0.15 V corresponds to the quasi reversible process.

3.8. Powder XRD

Powder XRD patterns of the complexes were recorded over a range of 2θ = 0-80°. The data showed that $[Co(SN\text{-}NNDMB)_2Cl_2]$, $[Ni(SN\text{-}NNDMB)_2Cl_2]$, $[Cu(SN\text{-}NNDMB)_2Cl_2]$, and $[Zn(SN\text{-}NNDMB)_2Cl_2]$ complexes cause sharp peaks indicating their crystalline nature. The average crystallite sizes of the complexes were calculated using Scherrer's formula. The complexes have an average crystallite size of 26–35 nm. Based on the above studies, the overall synthetic procedure and structure of the compounds are shown in Scheme 2.

4. Biological studies

4.1. Antimicrobial activity

The results of the antimicrobial activities are presented in Table 6. The experiment's standard error is ± 0.001 cm and the experiment was repeated thrice under similar conditions. DMSO was used as a negative control for the antibacterial studies and amikacin, ofloxacin and ciprofloxacin were used as positive standards. Nystatin was used as a reference for antifungal studies. These compounds exhibit moderate to intense antimicrobial activity. The copper(II) complex shows a remarkable activity, especially against Gram-negative bacteria such as *E. coli* and *B. subtilis*. The Cu complex shows better action against *E. coli* compared to the standard amikacin. The Zn complex displays a moderate activity against the bacteria as well as the fungal species *C. albicans*. The antimicrobial activity of the synthesized complexes is greater than that of the metal-free ligand, indicating that the complexation with metal enhances the activity of SN-NNDMB. This could be elaborated on the basis of the well-known Overtone concept and chelation theory [26]. Chelation tends to make the ligand SN-NNDMB more powerful and a potent antibacterial agent.

Table 5
Thrmogravimetric data of Schiff base metal complexes.

Complex	Temperature range T (°C)	% Weight loss Obs.(calcd)	Process
$[Co(SN\text{-}NNDMB)_2Cl_2]$	260–545 > 550	93.45 (93.05) 6.95 (6.95)	Loss of organic moiety CoO
$[Ni(SN\text{-}NNDMB)_2Cl_2]$	300–690 > 700	92.75 (93.06) 7.25 (6.94)	Loss of organic moiety NiO
$[Cu(SN\text{-}NNDMB)_2Cl_2]$	290–700 > 700	93.10 (92.70) 6.90 (7.3)	Loss of organic moiety CuO
$[Zn(SN\text{-}NNDMB)_2Cl_2]$	275–800 > 800	93.23 (92.52) 6.77 (7.48)	Loss of organic moiety ZnO

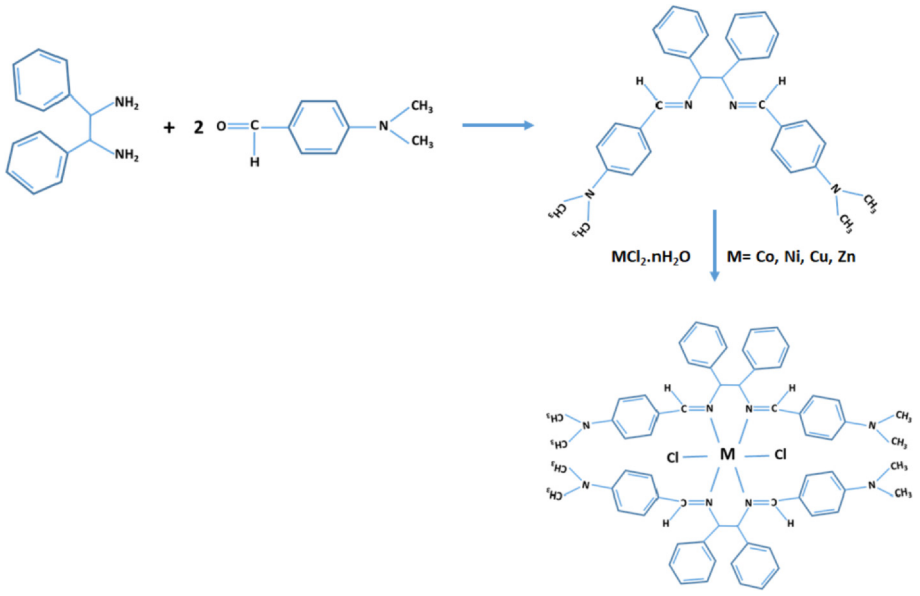

Scheme 2. The synthetic procedure of SN-NNDMB and its metal complexes.

Table 6
In vitro antimicrobial activity (MIC, μg/mL) of SN-NNDMB, complexes and standard reagents.

Compound	Bacterial species				Fungal species		
	E. coli	*B. subtilis*	*P. aeruginosa*	*S. aureus*	*A. niger*	*A. flavus*	*C. albicans*
SN-NNDMB	54	80	>100	68	28	>100	47
$[Co(SN\text{-}NNDMB)_2Cl_2]$	>100	>100	26	86	26	27	19
$[Ni(SN\text{-}NNDMB)_2Cl_2]$	28	32	21	31	43	>100	20
$[Cu(SN\text{-}NNDMB)_2Cl_2]$	03	07	14	22	08	18	06
$[Zn(SN\text{-}NNDMB)_2Cl_2]$	12	18	43	21	45	>100	09
Amikacin[a]	05	05	04	05	–	–	–
Ciprofloxacin[a]	05	05	05	05	–	–	–
Ofloxacin[a]	10	2.5	2.5	05	–	–	–
Nystatin[a]	–	–	–	–	06	06	05

[a] Standard.

4.2. DNA binding studies

4.2.1. Absorption titration method

The metal(II) complexes DNA binding ability was investigated by electronic absorption titration. This is an effective method to examine the binding mode of DNA to metal complexes. The intercalative mode of binding usually results in a hypochromism and redshift because of the strong stacking interaction between an aromatic chromophore and the base pairs of DNA. The extent of the spectral change is related to the binding strength. The electronic absorption titration of a Cu complex is shown in Fig. 3. The absorption band of the Co(II) complex at 368.6 nm exhibits a hypochromism of 7.6% and a bathochromism of 4.1 nm. The absorption band of the Ni(II) complex at 356.8 nm exhibits a hypochromism of 13.7% and a bathochromism of 2.3 nm. The absorption band of Cu complex at 384.8 nm exhibits a hypochromism of 20.01% and a bathochromism of 4.7 nm. The Zn complex at 372.4 nm shows a hypochromism of 4.6% and a bathochromism of 2.5 nm. These results suggest an association of the complexes with DNA and a interaction with DNA through intercalation. The intrinsic binding constant (K_b) values were also calculated and found to be 2.5×10^5, $3.2x\ 10^5$, $3.5x\ 10^5$ and $2.6x\ 10^5\ M^{-1}$ for the respective complexes Co(II), Ni(II), Cu(II) and Zn(II).

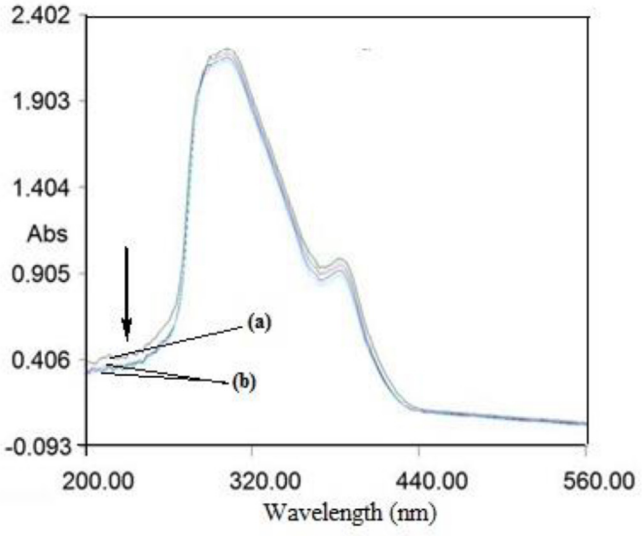

Fig. 3. The electronic absorption spectrum of a) $[Cu(SN\text{-}NNDMB)_2Cl_2]$ in the absence of CT DNA and b) in the presence of an increasing amount of CT DNA.

4.2.2. Viscosity measurements

A viscosity study further confirmed the interaction of the metal complexes with DNA. The viscosity measurement is based on the flow rate of a DNA solution through a capillary viscosimeter. The relative viscosity contribution (η) cause by the DNA in the presence of a binding agent was obtained. A classical intercalation model usually resulted in lengthening the DNA helix, as base pairs were separated to accommodate the binding ligand which leads to an increase of DNA viscosity. The viscosity of CT DNA increases with an increase in the ratio of complexes to CT DNA (Fig. 4). The result further suggests an intercalative binding mode of the complexes with CT DNA and, parallelled to the spectroscopic results above such as hypochromism, a blue-shift of complexes in the presence of DNA. The viscosity studies provide strong evidence for intercalation. The viscosity increase of DNA is attributed to the intercalative binding mode of the drug because this could cause the effective length of the DNA to increase [27].

4.3. DNA cleavage analysis

Gel electrophoresis experiments using CT DNA were performed with the ligand and its complexes in the presence or absence of the oxidant H_2O_2. The obtained results clearly indicate that all the complexes could interact with CT DNA in the presence of H_2O_2. All the complexes cleave DNA completely as shown in Fig. 5. The metal complexes seem to catalyze the generation of highly reactive hydroxyl radicals from H_2O_2. These hydroxyl radicals participate in the deoxyribose moiety oxidation, followed by the sugar-phosphate backbone hydrolytic cleavage. The complexes completely cleave the DNA by generating the hydroxyl radicals. Most cleavage cases are caused by the metal ions interacting with H_2O_2 to produce diffusible hydroxyl radicals or molecular oxygen, which may damage DNA through Fenton-type chemistry [28]. The nuclease activity of the complexes was also investigated in the absence of H_2O_2 but did not cleave the DNA, confirming the involvement of hydroxyl radicals in the cleavage process.

4.4. Antitubercular activity

Resazurin Microtiter Assay (REMA) was used to determin the antimicobacterial activity. The results presented in Table 7 indicate that the Schiff base ligand has no inhibition against *M. tuberculosis* H37Rv growth up to a 100 μM concentration. The reported Schiff base (SN-NNDMB) and the metal complexes except the Cu complex have no significant activity compared to commercial drugs. At 100 μM, the Cu complex inhibits the growth of tubercular bacteria. This complex starts to impede the development of the organism at a 100 μM concentration.

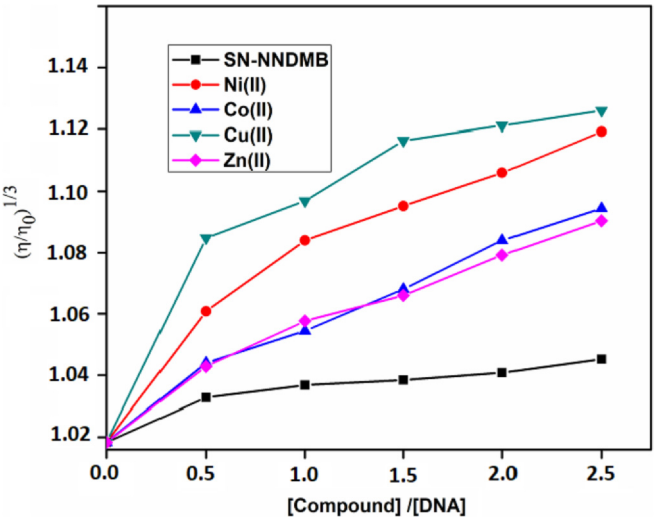

Fig. 4. Effect of increasing amount of SN-NNDMB and its metal complexes on the relative viscosity of CT-DNA.

4.5. Anticancer activity

In order to test the biological effects of the ligand SN-NNDMB and its Co(II), Ni(II), Cu(II), and Zn(II) complexes on cancer cells, the compounds were used to treat HCT116 (Colon Cancer Cells) and HeLa (Human Cervical Cancer Cells) at concentrations of 6.25, 12.50, 25.00, 50.00, and 100.00 μM for 48 h. Untreated cells were used as the control group. Cell growth inhibition was analyzed by MTT assay and the results revealed that the ligand and complexes exhibited a dose-dependent inhibitory effect on the proliferation of HCT116 and HeLa cells as shown in the Fig. 6a and b as well as Table 8. The IC_{50} values for the complexes Cu(II) and Zn(II) are very low compared to the other complexes and the free ligand (SN-NNDMB). This indicates that these compounds have pronounced anti-proliferative effects on HeLa and HCT116 cancer cells. Higher IC_{50} values were noticed for the cases of the Co(II) and Ni(II) complexes and the free ligand (SN-NNDMB) on both HeLa and HCT116 cancer cells. The IC_{50} values for Cu(II), Zn (II), Co(II), Ni(II) complexes for HeLa cancer cells are better than those for the HCT116 cancer cells. The IC_{50} values for the metal complexes prepared here and the unbound ligand against HCT116 cancer cells show moderate activities compared to the IC_{50} value of clinically used drugs such as etoposide (29.6 μM) [29]. Furthermore, the activity of the metal complexes and the free ligand (SN-NNDMB) towards HeLa cancer cells are not very significant compared to known metal-free anticancer agents such as estramustine (IC_{50} ~1.5 to 3.0 μM), [30] noscapine (IC_{50} ~22 μM), [31] or metal-bound anticancer reagents such as cisplatin (IC50 ~8 μM) [32]. From the IC_{50} values, the Cu(II) and Zn(II) complexes showed better activity on HCT116 cancer cells than on the HeLa cancer cells.

4.6. SOD mimetic activity

The SOD mimetic activity values (IC50) of the synthesized complexes are presented in Table 9. The data shows that the activity of the complexes is low compared to the native enzyme. The Cu complex has a higher activity than other complexes. In various complexes functioning as SOD enzymes, there is either a one-electron oxidation followed by the reduction of a metal ion or the formation of a superoxide complex, which then is reduced to a peroxide by another superoxide ion. In order to explore this mechanism, the absorption spectrum of complexes was recorded in the presence and absence of alkaline DMSO (alkaline DMSO acts as a source of O^{2-}). The spectrum peaks were suppressed in alkaline DMSO-containing a buffer (pH 8.6). However, adding NBT, which acts as O^{2-} scavenger, reverted these peaks to their original position. This indicates that O^{2-} is initially attached to the metal complex, which is later reduced by another O^{2-} ion. The scavenging ability of each complex gave its final concentration that produced an efficient quenching of the superoxide anion radical. In the present study, the Cu complex has a higher SOD mimetic activity than the other complexes. The IC_{50} value for the copper complex is lower than that of the other complexes and the free ligand.

5. Conclusion

Schiff base ligands derived from *meso*-1,2-diphenylethylenediamine (*meso*-stien) and 4-N,N′-dimethylaminobenzaldehyde (SN-NNDMB) and its transition complexes were synthesized. The struc-

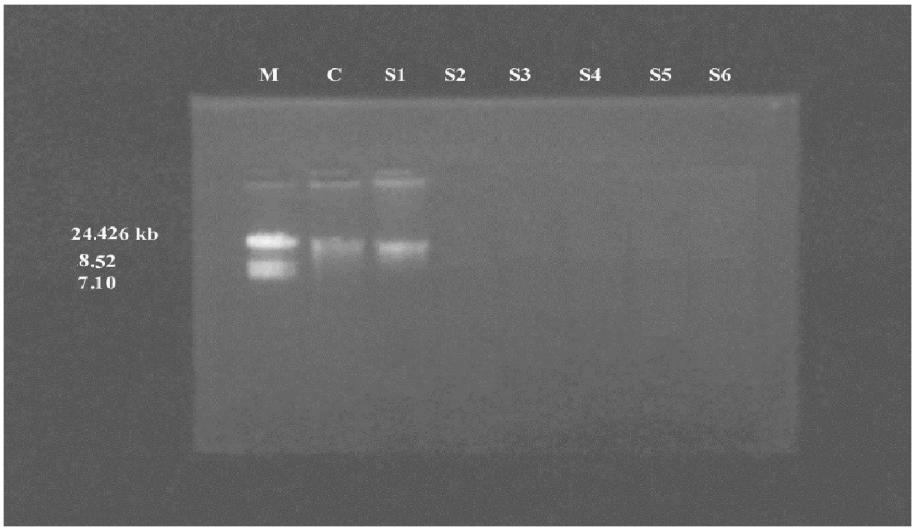

Fig. 5. DNA cleavage studies M- Marker, C- Control CT DNA (untreated sample), S1 – H_2O_2 + DNA, S2 – Ligand + H_2O_2 + DNA, S2 - [Co(SN-NNDMB)$_2$Cl$_2$] + H_2O_2 + DNA, S3- [Ni(SN-NNDMB)$_2$Cl$_2$] + H_2O_2 + DNA, S4 – [Cu(SN-NNDMB)$_2$Cl$_2$] + H_2O_2 + DNA, S5 – [Zn(SN-NNDMB)$_2$Cl$_2$] + H_2O_2 + DNA.

Table 7
Antimycobacterial activity of SN-NNDMB and its complexes.

Compound	100 μg/mL	50 μg/mL	25 μg/mL	12.5 μg/mL	6.25 μg/mL
SN-NNDMB	N	N	N	N	N
[Co(SN-NNDMB)$_2$Cl$_2$]	N	N	N	N	N
[Ni(SN-NNDMB)$_2$Cl$_2$]	N	N	N	N	N
[Cu(SN-NNDMB)$_2$Cl$_2$]	P	N	N	N	N
[Zn(SN-NNDMB)$_2$Cl$_2$]	N	N	N	N	N

N = No inhibition.
P = Inhibition

ture of the Schiff base ligand was verified by single-crystal XRD. From the spectral data, the Schiff base coordination to the metal atom was found to be through the azomethine nitrogen and the geometry of the complexes was found to be octahedral. The Cu (II) complex shows a better activity against Gram-negative bacteria such as *E-coli* then the other synthesized complexes. All synthesized complexes cleave DNA completely. From the DNA binding studies, it can be concluded that the compounds were interacting with CT-DNA through intercalation. The Cu(II) complex shows a comparable activity against both tested cancer cells. The Cu(II)

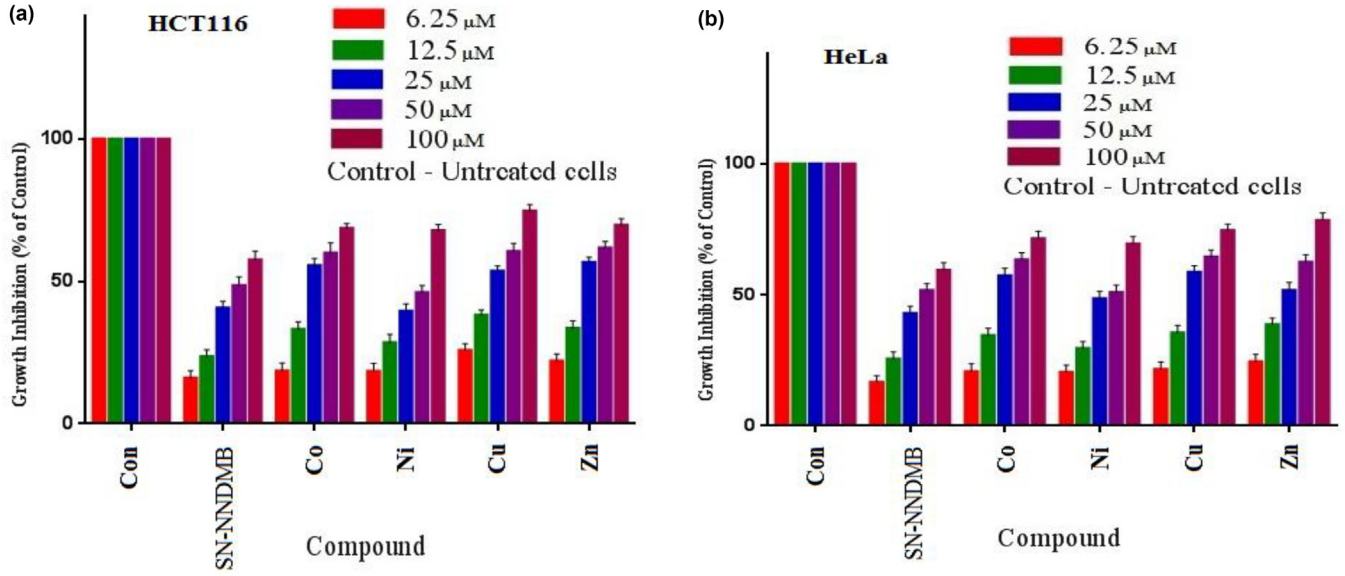

Fig. 6. a. The activity of compounds on HCT116 b. The activity of compounds on HeLa.

Table 8
IC_{50} values of SN-NNDMB and its complexes.

Compound	IC_{50} (μM)	
	HeLa	HCT116
SN-NNDMB	56.6	49.1
$[Co(SN\text{-}NNDMB)_2Cl_2]$	28.8	25.1
$[Ni(SN\text{-}NNDMB)_2Cl_2]$	46.3	36.5
$[Cu(SN\text{-}NNDMB)_2Cl_2]$	24.1	23.2
$[Zn(SN\text{-}NNDMB)_2Cl_2]$	26.5	24.5

Table 9
Superoxide dismutase activity of compounds (IC50 values).

Compounds	IC_{50} (mM)
SN-NNDMB	226
$[Co(SN\text{-}NNDMB)_2Cl_2]$	47
$[Ni(SN\text{-}NNDMB)_2Cl_2]$	64
$[Cu(SN\text{-}NNDMB)_2Cl_2]$	12
$[Zn(SN\text{-}NNDMB)_2Cl_2]$	72
Native SOD	6

complex also shows a good SOD-like activity compared to the other synthesized compounds.

CRediT authorship contribution statement

C. Shiju: Conceptualization, Methodology, Formal analysis, Investigation, Data curation, Writing - original draft, Writing - review & editing, Visualization. **D. Arish:** Conceptualization, Methodology, Validation, Formal analysis, Writing - original draft, Writing - review & editing, Visualization. **N. Bhuvanesh:** Crystallography studies. **S. Kumaresan:** Validation, Resources, Data curation, Writing - review & editing, Supervision, Project administration.

Declaration of Competing Interest

The authors declare that they have no known competing financial interests or personal relationships that could have appeared to influence the work reported in this paper.

Appendix A. Supplementary data

Supplementary data to this article can be found online at https://doi.org/10.1016/j.poly.2021.115292.

References

[1] X. Liu, J.-R. Hamon, Recent developments in penta-, hexa- and heptadentate Schiff base ligands and their metal complexes, Coord. Chem. Rev. 389 (2019) 94–118, https://doi.org/10.1016/j.ccr.2019.03.010.

[2] M. Ignatova, N. Stoyanova, N. Manolova, I. Rashkov, R. Kukeva, R. Stoyanova, R. Toshkova, A. Georgieva, Electrospun materials from polylactide and Schiff base derivative of Jeffamine ED® and 8-hydroxyquinoline-2-carboxaldehyde and its complex with Cu2+: preparation, antioxidant and antitumor activities, Mater. Sci. Eng. C 116 (2020), https://doi.org/10.1016/j.msec.2020.111185 111185.

[3] M. Tavassoli, M. Montazerozohori, R. Naghiha, H. Sadeghi, A. Masoudiasl, S. Joohari, E.V. Lopez, G. Mahmoudi, Some new nanostructure zinc complex: synthesis, spectral analyses, crystal structure, Hirshfeld surface analyses, antimicrobial/anticancer, thermal behavior and usage as precursor for ZnO nanostructure, Mater. Sci. Eng. C 110 (2020), https://doi.org/10.1016/j.msec.2020.110642 110642.

[4] R. Reshma, R. Selwin Joseyphus, D. Arish, L. John, Synthesis and spectral characterization of metal complexes of Schiff base derived from indole-3-carboxaldehyde and L-histidine as potent biocides, J. Coord. Chem., 72:19-21 (2019) 3326-3337. DOI: 10.1080/00958972.2019.1695126

[5] M.A. Malik, O.A. Dar, P. Gull, M.Y. Wani, A.A. Hashmi, Heterocyclic Schiff base transition metal complexes in antimicrobial and anticancer chemotherapy, Med. Chem. Commun. 9 (2018) 409–436, https://doi.org/10.1039/C7MD00526.

[6] T. Kondori, N. Akbarzadeh-T, M. Fazli, B. Mir, M. Dušek, V. Eigner, A novel schiff base ligand and its copper complex: Synthesis, characterization, X-ray crystal structure and biological evaluation, J. Mol. Struct. 1226 (2021), https://doi.org/10.1016/j.molstruc.2020.129395 129395.

[7] J. Zhang, L. Xu, W.-Y. Wong, Energy materials based on metal Schiff base complexes, Coord. Chem. Rev. 355 (2018) 180–198, https://doi.org/10.1016/j.ccr.2017.08.007.

[8] D. Kılınç, Ö. Şahin, Metal-Schiff Base complex catalyst in KBH_4 hydrolysis reaction for hydrogen production, Int. J. Hydrog. Energy 44 (2019) 18848–18857, https://doi.org/10.1016/j.ijhydene.2019.01.229.

[9] S. Shi, S. Yu, L. Quan, M. Mansoor, Z. Chen, H. Hu, D. Liu, Y. Liang, F. Liang, Synthesis and antitumor activities of transition metal complexes of a bis-Schiff base of 2-hydroxy-1-naphthalenecarboxaldehyde, J. Inorg. Biochem. 210 (2020), https://doi.org/10.1016/j.jinorgbio.2020.111173 111173.

[10] F. Hueso-Ureña, N. A.Illán-Cabeza, M.N. Moreno-Carretero, J.M. Martínez-Martos, M. J. Ramírez-Expósito, Synthesis and spectroscopic studies on the new Schiff base derived from the 1:2 condensation of 2,6-diformyl-4-methylphenol with 5-aminouracil (BDF5AU) and its transition metal complexes: Influence on biologically active peptides-regulating aminopeptidases, J. Inorg. Biochem.,94 (2003) 326-334. 10.1016/S0162-0134(03)00025-4

[11] H. Zhang, S. Gou, J. Zhao, F. Chen, G. Xu, X. Liu, Cytotoxicity profile of novel sterically hindered platinum(II) complexes with (1R,2R)-N^1, ^{N}2-dibutyl-1,2-diaminocyclohexane, Eur. J. Med. Chem. 96 (2015) 187–195, https://doi.org/10.1016/j.ejmech.2015.04.019.

[12] J.S. Saad, M. Benedetti, G. Natile, L.G. Marzilli, Basic Coordination Chemistry Relevant to DNA Adducts Formed by the Cisplatin Anticancer Drug. NMR Studies on Compounds with Sterically Crowded Chiral Ligands, Inorg. Chem., 49 (12) (2010) 5573-5583. DOI: 10.1021/ic100494f

[13] K. Sundaravel, E. Suresh, M. Palaniandavar, Synthesis, structures, spectral and electrochemical properties of copper(II) complexes of sterically hindered Schiff base ligands, Inorganica Chim. Acta 362 (2009) 199–207, https://doi.org/10.1016/j.ica.2008.03.083.

[14] J.E. Baumeister, A.W. Mitchell, S.P. Kelley, C.L. Barnes, S.S. Jurisson, Steric influence of salicylaldehyde-based Schiff base ligands on the formation of trans-$[Re(PR_3)_2(Schiff\ base)]^+$ complexes, Dalton Trans. 48 (2019) 12943–12955, https://doi.org/10.1039/C9DT02630D.

[15] B. Biannic, J.J. Bozell, T. Elder, Steric effects in the design of Co-Schiff base complexes for the catalytic oxidation of lignin models to *para*-benzoquinones, Green Chem. 16 (2014) 3635–3642, https://doi.org/10.1039/C4GC00709C.

[16] E. Tas, M. Aslanoglu, M. Guler, M. Ulusoy, Synthesis, characterization and electrochemical properties of copper(II) complexes with novel bidentate salicylaldimines derived from 3,5-di-t-butyl-2-hydroxybenzaldehyde, J. Coord. Chem. 57 (7) (2004) 583–589, https://doi.org/10.1080/00958970410001697239.

[17] R. Savka, M. Bergmann, Y. Kanai, S. Foro, H. Plenio, Triptycene-Based Chiral and meso-N-Heterocyclic Carbene Ligands and Metal Complexes, Chem. Eur. J. 22 (2016) 9667–9675, https://doi.org/10.1002/chem.201601474.

[18] A.R. Khokhar, G.J. Lumett, Synthesis and characterization of A series of Platinum(II) and Palladium(II) complexes containing the bidentate ligand meso-1,2-Diphenylethylenediamine OR meso-1,2-Bis(4- Chlorophenyl) Ethylenediamine, J. Coord. Chem. 19 (4) (1989) 321–330, https://doi.org/10.1080/00958978909408835.

[19] C. Shiju, D. Arish, N. Bhuvanesh, S. Kumaresan, Synthesis, characterization, and biological evaluation of Schiff base–platinum(II) complexes, Spectrochim. Acta A Mol Biomol. Spectrosc. 145 (2015) 213–222, https://doi.org/10.1016/j.saa.2015.02.030.

[20] C. Shiju, D. Arish, S. Kumaresan, Novel water soluble Schiff base metal complexes: Synthesis, characterization, antimicrobial-, DNA cleavage, and anticancer activity, J. Mol. Struct. 1221 (2020), https://doi.org/10.1016/j.molstruc.2020.128770 128770.

[21] C. Shiju, D. Arish, S. Kumaresan, Synthesis, characterization, cytotoxicity, DNA cleavage, and antimicrobial activity of lanthanide(III) complexes of a Schiff base ligand derived from glycylglycine and 4-nitrobenzaldehyde, Arab. J. Chem. 10 (2017) S2584–S2591, https://doi.org/10.1016/j.arabjc.2013.09.036.

[22] A. Martin, M. Camacho, F. Portaels, J.C. Palomino, Resazurin microtiter assay plate testing of Mycobacterium tuberculosis susceptibilities to second-line drugs: rapid, simple, and inexpensive method, Antimicrob. Agents Chemother. 47 (2003) 3616, https://doi.org/10.1128/aac.47.11.3616-3619.2003.

[23] A. Martin, J.C. Palomino, Resazurin Microtiter Assay (REMA) : Resazurin Microtitre assay (REMA) Colorimetric redox indicator (CRI). Drug susceptibility testing for Mycobacterium tuberculosis, Institute of Tropical Medicine, Belgium. Procedure manual Version 03-2009.

[24] A. B. P. Lever: Inorganic Electronic Spectroscopy, Vol. 33 aus: Studies in Physical and Theoretical Chemistry, Elsevier, Amsterdam, Oxford, New York, Tokio 1984.

[25] D. Banerjea, Coordination Chemistry, Tata McGraw-Hill Pub, (1993).

[26] A. Leite, L.J. Bessa, A.M.G. Silva, P. Gameiro, B. de Castro, M. Rangel, Antibacterial activity of naphthyl derived *bis*-(3-hydroxy-4-pyridinonate) copper(II) complexes against multidrug-resistant bacteria, J. Inorg. Biochem. 197 (2019), https://doi.org/10.1016/j.jinorgbio.2019.110704 110704.

[27] B.S. Rajebhosale, S.N. Dongre, S.S. Deshpande, A.N. Kate, A.A. Kumbhar, Aryl-1H-imidazole[4,5*f*][1,10]phenanthroline Cu(II) complexes: electrochemical and DNA interaction studies, J. Inorg. Biochem. 175 (2017) 129–137, https://doi.org/10.1016/j.jinorgbio.2017.07.008.

[28] V. Uma, M. Kanthimathi, T. Weyhermuller, B.U. Nair, Oxidative DNA cleavage mediated by a new copper (II) terpyridine complex: Crystal structure and DNA binding studies, J. Inorg. Biochem. 99 (2005) 2299–2307, https://doi.org/10.1016/j.jinorgbio.2005.08.011.
[29] M.A. LeBlanc, A.G. Sarrias, F.A. Beckford, P.M. barushimana, and N.P. Seeram, Coordination Chemistry of Polyaromatic Thiosemicarbazones 2: Synthesis and Biological Activity of Zinc, Cobalt, and Copper Complexes of 1-(Naphthalene-2-yl)ethanone Thiosemicarbazone, Int. J. Inorg. Chem, (2011) 8. 10.1155/2011/624756.
[30] K.M. Nicholson, R.M. Phillips, S.D. Shnyder, M.C. Bibby, *In vitro* and *in vivo* activity of LS 4477 and LS 4559, novel analogues of the tubulin binder estramustine, Eur. J. Cancer 38 (2002) 194, https://doi.org/10.1016/S0959-8049(01)00341-0.
[31] J. Zhou, K. Gupta, S. Aggarwal, R. Aneja, R. Chandra, D. Panda, C.H. Joshi, Brominated derivatives of noscapine are potent microtubule-interfering agents that perturb mitosis and inhibit cell proliferation, Mol. Pharmacol 63 (2003) 799, https://doi.org/10.1124/mol.63.4.799.
[32] S. Ray, R. Mohan, J.K. Singh, M.K. Samantaray, M.M. Shaikh, D. Panda, P. Ghosh, Anticancer and antimicrobial metallopharmaceutical agents based on palladium, gold, and silver N-heterocyclic carbene complexes, J. Am. Chem. Soc 129 (2007) 15042, https://doi.org/10.1021/ja075889z.